Theory of ballistic-electron-emission microscopy of buried semiconductor heterostructures

D. L. Smith and Sh. M. Kogan
Los Alamos National Laboratory, Los Alamos, New Mexico 87545
(Received 23 April 1996)

We extend the theoretical description of ballistic-electron-emission microscopy (BEEM) to the study of buried heterojunctions. We calculate the collector current and its first and second derivatives with respect to tip-base bias voltage for buried single-barrier and double-barrier resonant tunneling structures and show how they systematically vary with the parameters of the heterostructure. We show that the second derivative of the collector current is approximately a product of the heterostructure transmission coefficient and a slowly varying function of bias voltage. The calculated results are in good agreement with the first measurements of BEEM used to probe buried double-barrier heterostructures. [S0163-1829(96)09839-6]

Ballistic-electron-emission microscopy (BEEM) has been shown to have unique capabilities to probe metal/semiconductor interfaces with nanometer resolution.[1–10] Very recently BEEM techniques have been extended to the study of buried semiconductor heterostructures[11] including single-barrier and double-barrier resonant tunneling structures (DBRTS). In Ref. 11, it was shown that BEEM is a powerful probe of heterostructures because the electron energy distribution incident on the heterostructure can be varied independently of the energy-band profile. In conventional heterojunction device structures, both the incident electron energy distribution and the energy-band profiles of the heterostructure change with bias voltage. In Ref. 11, second derivatives of the collector current with respect to voltage bias were shown to yield peaked structure which could be associated with the various heterostructure transmission channels and thus provide a spectroscopic study of heterostructure transmission. The purpose of this paper is to extend the theoretical description of BEEM to the study of buried heterostructure to help interpret the results of this new spectroscopic tool.

Figure 1 shows the schematic energy-band diagram of BEEM used as a probe of buried heterostructures. The dashed box to the left represents the scanning tunneling microscope (STM) tip with Fermi energy E_f and work function Φ. To the right of the STM tip is a thin vacuum region followed by a base region formed by a thin metal layer on the surface of the semiconducting sample. To the right of the base is a drift region formed by a capping layer of the semiconductor sample. The drift region is thin compared to an electron mean free path. The Schottky barrier between the base and drift regions is E_S. The heterostructure to be studied, in this schematic a DBRTS with energy barriers E_b, follows the drift region. To the right of the heterostructure is a collecting region. A δ-doping layer in the collector region is used to keep the bands flat in the drift and heterostructure regions and to provide a collecting field.[11] Electrons injected from the STM tip into the drift region are transmitted or reflected at the heterostructure. Transmitted electrons are collected by the field from the δ-doping layer and yield a collector current. Reflected electrons are captured in the base region and contribute to the base current. The distance between the tip and the base is adjusted to keep the base tunneling current constant and the collector current is measured as a function of tip voltage.

BEEM has been described using a planar tunneling model in which the STM tip and the base are modeled as planar films of free electron metals.[1–5] Other theoretical approaches which relax parallel wave-vector conservation[6,7] or which utilize first-principles description of the metal/semiconductor interface[10] have also been presented. Here we work within the context of the planar tunneling model. In the planar tunneling model, tunneling current to the base is calculated using the WKB approximation. The tunneling electrons in the base which traverse the base/semiconductor interface determine the BEEM current. For simple metal/semiconductor structures, all the electrons which pass into the semiconductor contribute to the BEEM current. Here we consider the case in which there is a buried heterostructure in the semiconductor and only those electrons which pass into the semiconductor drift region and are also transmitted by the heterostructure contribute to the collector current. In this case, the collector current can be written as a product of the electron flux distribution in the drift region in front of the heterostructure and the transmission coefficient of the heterostructure,

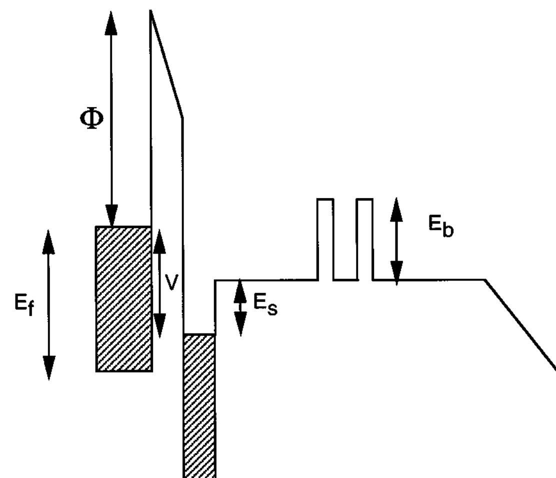

FIG. 1. Schematic energy band diagram of BEEM as a probe of buried heterostructures.

 © 1996 The American Physical Society

$$I_c(V)=eA\sum_{\mathbf{k}^d} F(\mathbf{k}^d,V)T(\mathbf{k}^d), \quad (1)$$

where I_c is the collector current, V is the magnitude of the bias voltage, e is the magnitude of the electron charge, A is the area in the planar tunneling model, $\mathbf{k}^d$ is the wave vector of an electron in the drift region (a sum on spins is included in the wave-vector sum), F is the electron flux distribution in the drift region, and T is the transmission coefficient of the heterostructure. If there is no heterostructure (T is unity) this expression reduces to the usual expression for the BEEM current. Equation (1) assumes that multiple scattering between the heterostructure and the base/drift interface is not important.

The flux distribution is found by multiplying the flux distribution of electrons that impinge on the surface of the STM tip by the transmission coefficient for tunneling to the base, the probability for traversing the base ballistically and the transmission coefficient at the base/drift interface

$$F(\mathbf{k}^d,V)=\sum_{\mathbf{k}^t,\mathbf{k}^b}\left[\Theta(k_\perp^t)\,\frac{f^t(\mathbf{k}^t)}{\nu}\,\frac{\hbar}{m}\,k_\perp^t\right]\times\{[1-f^b(\mathbf{k}^b)]e^{-2gl}\delta_{\mathbf{k}^b,\mathbf{k}^{b_0}(\mathbf{k}^t)}\}[e^{-\delta_b/\xi}]\Gamma_{\mathbf{k}^b,\mathbf{k}^d}, \quad (2)$$

where $\mathbf{k}^t$, $\mathbf{k}^b$, and $\mathbf{k}^d$ are wave vectors in the tip, base, and drift regions, respectively, Θ is the step function, f^t and f^b are Fermi distribution functions in the tip and base, respectively, ν is the normalization volume of the tip, l is the thickness of the vacuum region, the Kronecker delta ensures energy and interface parallel wave vector conservation for vacuum tunneling, δ_b is the thickness of the base, ξ is the ballistic path length in the base, the WKB factor g is

$$g=\sqrt{\alpha}\left\{\frac{2\alpha}{3\beta}\left[\left(1+\frac{\beta}{2\alpha}\right)^{3/2}-\left(1-\frac{\beta}{2\alpha}\right)^{3/2}\right]\right\}$$

where

$$\alpha=\frac{2m}{\hbar^2}\left[\Phi+E_f-\frac{eV}{2}-\frac{(\hbar k_\perp^t)^2}{2m}\right] \quad \text{and} \quad \beta=\frac{2m}{\hbar^2}\,eV,$$

and $\Gamma_{\mathbf{k}^b,\mathbf{k}^d}$ is the transmission coefficient for an electron with wave vector $\mathbf{k}^b$ in the base to wave vector $\mathbf{k}^d$ in the drift region. The first factor in square brackets on the right side of Eq. (2) is the flux distribution in the tip, the second factor is the transmission coefficient for tunneling to the base, the third term gives the probability for traversing the base ballistically, and the fourth term is the transmission coefficient at the base/drift interface.

We consider small voltage biases for GaAs/$Ga_xAl_{1-x}As$ structures where only the electrons in the Γ valley can contribute and describe the semiconductor drift region and heterostructure using the nonparabolic energy-dependent effective-mass model where the effective mass has the form[12]

$$m^*(E)=m^*\left(1+\frac{E}{E_g}\right),$$

where m^* is the band-edge effective mass and E_g is the energy gap. In the original theory of BEEM,[2] $\Gamma_{\mathbf{k}^b,\mathbf{k}^d}$ was

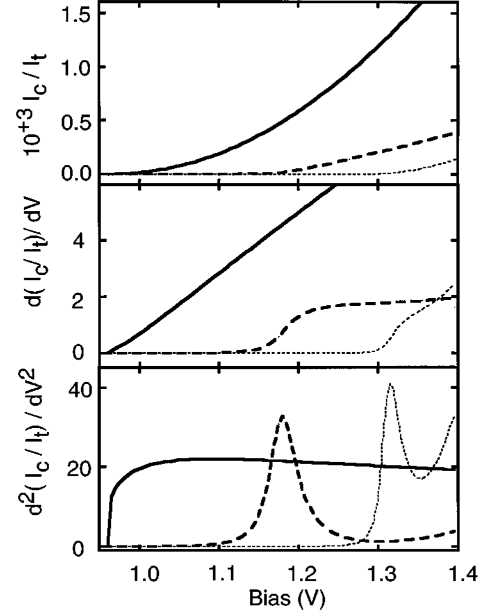

FIG. 2. Normalized collector current (upper panel), first (middle panel, units 10^{-3}/V), and second (lower panel, units $10^{-3}/V^2$) voltage derivatives of the normalized collector current with no heterostructure (solid line), the DBRTS (dashed line), and the single barrier (dotted line).

taken to be $\delta_{\mathbf{k}^d,\mathbf{k}^{d_0}(\mathbf{k}^b)}$, that is, unity if $\mathbf{k}^d$ satisfies energy and parallel wave-vector conservation conditions and zero otherwise. Here we include quantum-mechanical reflection at the base/drift interface[3–5] so that flux is conserved at that interface,

$$\Gamma_{\mathbf{k}^b,\mathbf{k}^d}=\frac{4(m_d/m)k_\perp^b k_\perp^d}{[(m_d/m)k_\perp^b+k_\perp^d]^2}\;\delta_{\mathbf{k}^d,\mathbf{k}^{d_0}(\mathbf{k}^b)},$$

where m^d is the energy-dependent effective mass in the drift region. The heterojunction transmission coefficient is calculated using the method of Ref. 13. Evaluating the integrals at zero temperature, Eq. (1) reduces to

$$I_c=eA\int_0^{eV-E_S}dE_\perp^d\int_{E_\perp^d}^{eV-E_S}dE^dF(E^d,E_\perp^d,V)T(E^d,E_\perp^d) \quad (3)$$

where

$$F(E^d,E_\perp^d,V)=\left(\frac{1}{(2\pi)^2}\,\frac{2m_d}{\hbar^3}\,e^{-\delta_b/\xi}\right)\times e^{-2gl}\left(\frac{4(m_d/m)k_\perp^{b_0}k_\perp^{d_0}}{[(m_d/m)k_\perp^{b_0}+k_\perp^{d_0}]^2}\right).$$

Here $E_\perp^d=(\hbar k_\perp^{d_0})^2/2m_d$, $E^d=(\hbar k^{d_0})^2/2m_d$, and the wave vector $k_\perp^{b_0}$ in the base is determined from $E_\perp^d$ and E^d by energy and interface parallel wave-vector conservation. We select parameters appropriate for a Au tip and base, E_f equals 5.5 eV and Φ equals 5.1 eV, a GaAs drift region, m_d^* equals 0.067m and heterojunction barriers made from $Al_{0.42}Ga_{0.58}As$, E_b equals 0.325 eV, and m^* equals 0.102m.

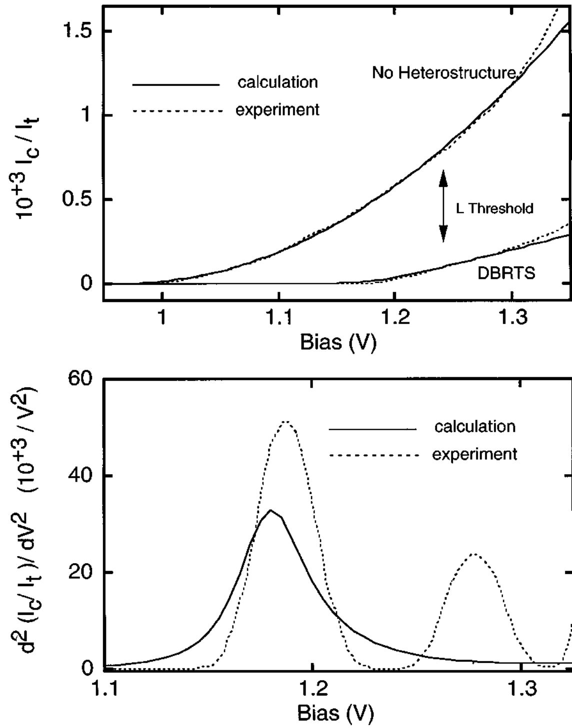

FIG. 3. Comparison between the measured (dotted line, from Ref. 11) and calculated (solid line) normalized collector current without a heterostructure and with the DBRTS (upper panel) and the second voltage derivative of the collector current with the DBRTS (lower panel).

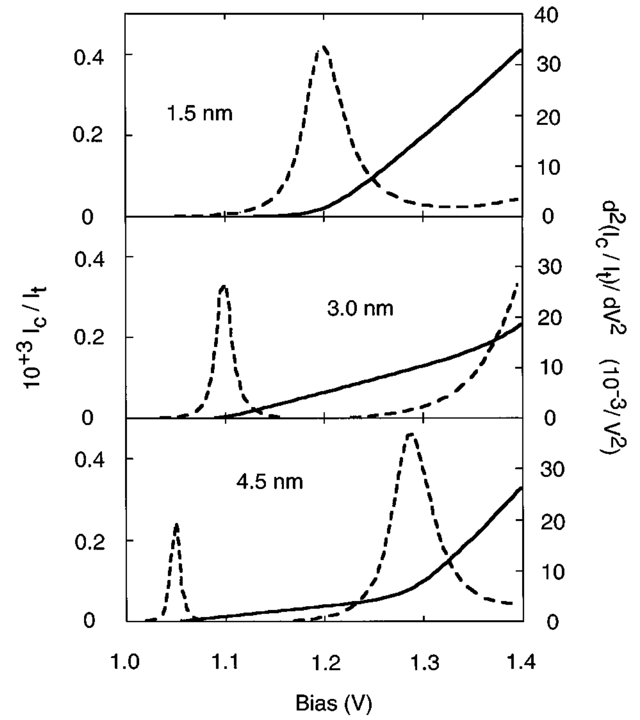

FIG. 4. Normalized collector current (solid lines) and second voltage derivative of the normalized collector current (dashed lines) for DBRTS with a 1.5-nm (upper panel), 3.0-nm (middle panel) and 4.5-nm (lower panel) quantum well.

The inelastic attenuation factor $e^{-\delta_b/\xi}$ and the Schottky barrier at the base/drift interface are fit to the experimental results of Ref. 11 when there is no heterostructure so that T is unity (0.0783 and 0.955 eV, respectively, were the fitting values). The thickness of the vacuum tunneling region l is adjusted so that the base tunneling current is fixed at 2 A/cm^2 for each voltage bias. This gives values for l which depend slightly on bias but are near 1 nm.

The upper panel of Fig. 2 shows the calculated collector current normalized to the base tunneling current as a function of bias voltage for no heterostructure barrier (solid line), the 2.3/1.7/2.3 nm DBRTS (dashed line) and the 10-nm single barrier (dotted line) which were studied experimentally in Ref. 11. The middle and lower panels show the first (units, 10^{-3}/V) and second (units, 10^{-3}/V^{-2}) derivatives, with respect to bias voltage, of the normalized collector currents, respectively. The second derivative curves in the lower panel of Fig. 2 closely resemble the transmission coefficients of the DBRTS and the single-barrier heterostructure. To understand this, we take the second derivative with respect to bias voltage taken of Eq. (3). The primary voltage dependence of Eq. (3) is due to the integration limits so its second derivative becomes

$$\frac{d^2I_c(V)}{d(eV)^2}=eA\left[\frac{1}{(2\pi)^2}\,\frac{2m_d}{\hbar^3}\,e^{-\delta_b/\xi}\right]\times\left[e^{-2gl}\left(\frac{4(m_d/m)k_\perp^{d_0}k_\perp^{b_0}}{[(m_d/m)k_\perp^{b_0}+k_\perp^{d_0}]^2}\right)\right]T+\text{small terms},\tag{4}$$

where all functions of $E_\perp^d$ or E^d are evaluated at $(eV-E_S)$. Except for very close to $eV=E_S$, the factor in front of the transmission coefficient is a slowly varying function of eV. Thus the second derivative of the collector current is approximately the heterostructure transmission coefficient modulated by a slowly varying function and is therefore a particularly interesting quantity in the study of heterostructures. This result provides a specific motivation for investigating the second derivative of the collector current.

In the upper panel of Fig. 3 we compare the calculated collector current normalized to the base tunneling current as a function of bias voltage for no heterostructure (i.e., the conventional BEEM result) and for the 2.3/1.7/2.3 nm DBRTS with the measured results of Ref. 11 at 77 K. The inelastic attenuation factor and the Schottky barrier at the base/drift interface were fit to the conventional BEEM data without a heterostructure but there were no additional adjustable parameters in the DBRTS heterostructure calculation. The lower panel compares the calculated second derivatives for the DBRTS heterostructure with the measured results of Ref. 11. The calculation agrees quite well with the DBRTS data for bias voltages below about 1.3 V and describes fairly well the first peak in the second derivative spectrum which results from tunneling through the resonant level in the DBRTS structure with no parameters adjusted for the DBRTS result. The agreement between the calculated and measured results for the DBRTS at bias below 1.3 V and for the lowest bias peak in the second derivative spectrum verifies the assignment in Ref. 11 that this current and peak are due to transmission through the resonant level of the DBRTS. At bias voltages greater than about 1.25 V transmission into the L valleys of GaAs becomes energetically

possible (parallel wave-vector conservation must be broken for transmission into the L valleys). For both the conventional BEEM data without a heterostructure and for the DBRTS heterostructure, there is additional current in the experiment that is not reproduced by the model, which does not include transmission into the L valleys, at voltages greater than about 1.3 V. An additional peak is seen in the second derivative spectrum at a bias of about 1.27 V. Because the additional current and peak in the second derivative spectrum occur at voltages that correspond to the GaAs L valley energy, they most likely result from transmission into these valleys.

In Fig. 4, we show the calculated normalized collector current and second-derivative of the normalized collector current as a function of bias voltage for a series of DBRTS in which the width of the quantum well has been increased from 1.5 to 3.0 to 4.5 nm. In all cases the barriers are 2.3 nm wide and 0.325 eV high. For the 1.5-nm well DBRTS, there is a single, relatively wide peak in the second derivative curve that results from transmission through the resonant level of the structure. As the width of the well is increased, this peak moves to lower voltages and narrows. A second resonant peak show up as the well is further increased to 4.5 nm. This result predicts how the collector current varies systematically with the parameters of the heterostructure.

For semiconductor heterostructures whose transmission properties are unknown, the application of BEEM techniques can provide a powerful method to study these transmission properties. $GaAs/Ga_xAl_{1-x}As$ heterostructures have been studied by other methods and much is known about their transmission properties. These heterostructures can be used as filters on the electron flux distribution to better characterize the BEEM process.

We have extended the theoretical description of BEEM to the study of buried heterojunctions. We have shown how the collector current and its bias voltage derivatives systematically varies with the parameters of the heterostructure. The calculated results are in good agreement with the measurements of Ref. 11 for low bias voltages where the Γ valley dominates the transport.

We thank Professor V. Narayanamurti for extremely useful discussions. The work was supported by the Los Alamos National Laboratory LDRD program.

[1] W. J. Kaiser and L. D. Bell, Phys. Rev. Lett. **60**, 1406 (1988).
[2] L. D. Bell and W. J. Kaiser, Phys. Rev. Lett. **61**, 2368 (1988).
[3] M. Prietsch and R. Ludeke, Phys. Rev. Lett. **66**, 2511 (1991).
[4] H. D. Hallen, A. Fernandez, T. Huang, J. Silcox, and R. A. Buhrman, Phys. Rev. B **46**, 7256 (1992).
[5] G. N. Henderson, P. N. First, T. K. Gaylord, and E. N. Glytsis, Phys. Rev. Lett. **71**, 2999 (1993).
[6] L. J. Schowalter and E. Y. Lee, Phys. Rev. B **43**, 9308 (1991).
[7] R. Ludeke and A. Bauer, Phys. Rev. Lett. **71**, 1760 (1993).
[8] J. J. O'Shea, T. Sajoto, S. Bhargava, D. Leonard, M. A. Chin, and V. Narayanamurti, J. Vac. Sci. Technol. B **12**, 2625 (1994).
[9] W. J. Kaiser, M. H. Hecht, L. D. Bell, F. J. Grunthaner, J. K. Liu, and L. C. Davis, Phys. Rev. B **48**, 18 324 (1993).
[10] M. D. Stiles and D. R. Hamann, Phys. Rev. Lett. **66**, 3179 (1991).
[11] T. Sajoto, J. J. O'Shea, S. Bhargava, D. Leonard, M. A. Chin, and V. Narayanamurti, Phys. Rev. Lett. **74**, 3427 (1995).
[12] B. K. Ridley, Solid State Electron. **24**, 147 (1981).
[13] D. J. Ben-Daniel and C. B. Duke, Phys. Rev. **152**, 683 (1966).